JOURNAL OF SPACECRAFT AND ROCKETS
Vol. 29, No. 2, March-April 1992

Viscous Supersonic Flow Computations over a Delta-Rectangular Wing with Slanting Surfaces

John S. Chan*
Boeing Aerospace & Electronics, Seattle, Washington 98124

A three-dimensional Navier-Stokes code has been applied to calculate flowfields over a sharp-edged delta-rectangular wing with slanting surfaces at supersonic conditions. The steady-state solutions were obtained by solving the full compressible Reynolds-averaged Navier-Stokes equations on a three-dimensional multizone grid using the MacCormack finite-volume explicit algorithm and the Baldwin-Lomax turbulence model. The computations were carried out at a fixed freestream Mach number and at various angles of attack. Grid resolution effects were also investigated. The numerical computations were found to agree well with the experimental data.

Nomenclature

b = wing semispan
C_L = lift coefficient, lift/qS
C_p = pressure coefficient, $2(p - p_\infty)/\gamma p_\infty M_\infty^2$
c_p = specific heat at constant pressure
i,j,k = indices of grid points in ξ, η, and ζ directions, respectively
k = coefficient of thermal conductivity, $k_L + k_T$
k_L = laminar thermal conductivity
k_T = turbulent thermal conductivity, $c_p\mu_T/Pr_T$
L = maximum longitudinal length of the wing
M = Mach number
M_∞ = freestream Mach number
Pr_T = turbulent Prandtl number
p = static pressure
p_T = total pressure
p_∞ = freestream static pressure
q = freestream dynamic pressure, $\rho_\infty U_\infty^2/2$
Re = Reynolds number based on L, $\rho_\infty U_\infty L/\mu_{L_\infty}$
S = wing planform area
U_∞ = freestream total velocity
u,v,w = Cartesian velocity components
x,y,z = Cartesian coordinates
y^+ = law-of-the-wall coordinate
α = angle of attack
γ = ratio of specific heats
μ = coefficient of viscosity, $\mu_L + \mu_T$
μ_L = laminar viscosity
μ_T = turbulent viscosity
ξ,η,ζ = computational body-fitted coordinates
ρ = density
ρ_∞ = freestream density

Introduction

COMPUTATIONAL fluid dynamics (CFD) has recently made great progress due to advances in computer hardware and algorithm development. Many complex engineering problems can be analyzed numerically using Euler or Navier-Stokes solvers. One of these engineering applications is performance prediction in aerospace vehicle design using a Navier-Stokes code. It commonly involves the calculation of viscous flowfields over three-dimensional wings by solving the full compressible Reynolds-averaged Navier-Stokes equations.

Experimental data[1-4] and numerical solutions[5-14] have shown that flow separation and vortex formation typify flow around three-dimensional sharp-edged delta wings. The flow separation near the leading edge and the subsequent formation of primary and secondary vortices above the leeside wing surface at moderate-to-high angles of attack result in nonlinear variation in lift. Vortex breakdown and the movement of the breakdown location due to the change in angle of attack at high setting would bring about a loss in lift and a nose-up pitching moment. Increases in the complexity of the wing geometry further complicate the flowfield around the wing because of the potential vortex interaction induced by the geometry.

In order to predict accurately the aerodynamic performance, the vortical flowfield around a wing should be well understood through either wind-tunnel testing or CFD calculation. The inability of Euler solvers to capture the secondary vortices over the leeside wing surface at high angle of attack necessitates the usage of Navier-Stokes codes in the CFD simulation of the flows. The complexities of the flowfield and the wing geometry, however, pose a great challenge to the development and application of new Navier-Stokes codes. The inclusion of slanting surfaces, for example, may significantly alter the flowfields discussed earlier for wings with only flat surfaces due to the existence of compression and expansion waves at the surface intersections. Validating the code by comparing the numerical solutions with experimental data is essential in order to make the CFD method a truly complementary engineering tool to wind-tunnel testing.

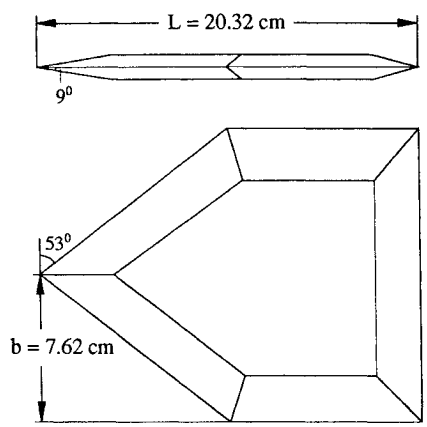

Fig. 1 Delta-rectangular wing geometry.

Received Dec. 28, 1989; presented as Paper 90-0419 at the AIAA 28th Aerospace Sciences Meeting, Reno, NV, Jan. 8-11, 1990; revision received May 14, 1990; accepted for publication May 23, 1990.

*Principal Engineer; currently at Boeing Commercial Airplane Group. Member AIAA.

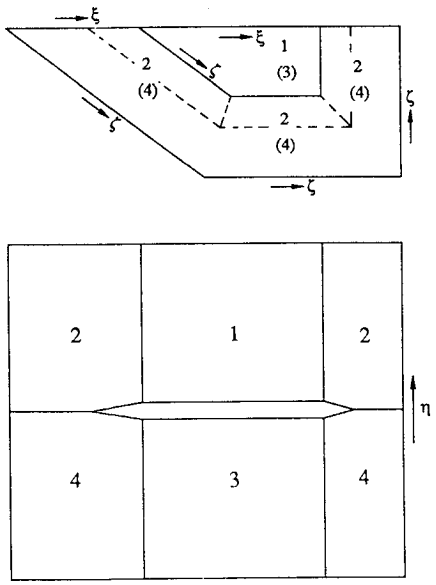

Fig. 2 Zonal grid arrangement.

A new three-dimensional Navier-Stokes code is being developed for a range of applications.[15-20] The code is based on the MacCormack explicit/implicit algorithm[21,22] and has multizone and multiple machine capabilities. For the purpose of validating the code and investigating the flow phenomena over a wing with slanting surfaces,[23] this code has been applied, using only the explicit scheme,[21] in the calculation of flowfields over a complex delta-rectangular wing: a rectangular wing with sharp, swept leading edges and several slanting surfaces (Fig. 1). In the computations, a multizone numerical approach and a Baldwin-Lomax turbulence model[24] were used. This paper summarizes the results of the computations at M_∞ = 2.16 and α = 1.3, 6.3, and 11.3 deg. The computational grid effect on the solution at α = 1.3 deg is also reported. The calculations were validated by comparing the numerical results with the test data of Ref. 23.

Wing Geometry and Computational Grids

The wing modeled in the computations was chosen from several used in the 1981 wing-alone supersonic aerodynamic characteristic wind-tunnel tests at NASA Langley Research Center.[23] It consists of two components: a delta section upstream with a 53-deg sweep and a 10.16- × 15.24-cm rectangular section downstream (Fig. 1). The maximum longitudinal and semispan lengths L and b are 20.32 and 7.62 cm, respectively. All the edges around the wing have a nominal zero thickness that increases to its maximum value of 1.27 cm through five slanting surfaces on each side of the wing. The wing has an aspect ratio of 2.0, a taper ratio of 0.5, and a half angle of 9 deg.

The body-fitted computational multizone grid was generated around the symmetrical half of the wing by a grid generator using a parabolic/elliptic algorithm.[25] The grid consists of four zones with zones 1 and 2 covering the computational domain over the leeward side of the wing and zones 3 and 4 the computational domain over the windward side. The wing geometry requires the zonal grid arrangement, shown in Fig. 2, in which zone 2 (or 4) is wrapped around zone 1 (or 3). This results in a region where one boundary in the ξ direction of one zone has to match with another boundary in the ζ direction of another zone.

The three-dimensional overall view of the grid is shown in Fig. 3. It can be seen that the grid points are clustered around the leading and trailing edges, as well as the surface intersections, in order to capture the flowfield details there. In the direction normal to the surfaces, the grid was clustered near the surfaces in order to resolve the turbulent boundary layer.

Table 1 Computational grids used in the calculations

Grid	Zones 1 & 3 $i \times j \times k$	Zones 2 & 4 $i \times j \times k$	Surface points	Minimum $\Delta\eta/L$
Coarse	21 × 34 × 15	15 × 34 × 49	2 × 658	1.3×10^{-4}
Medium	44 × 34 × 32	32 × 34 × 106	2 × 3740	1.3×10^{-4}
Fine	44 × 40 × 32	32 × 40 × 106	2 × 3740	0.3×10^{-4}

To study grid effects, calculations were performed using three grids with 71,400, 326,400, and 384,000 total grid points, respectively. Both the first and second grids, designated as the coarse and medium grids, respectively, have the same grid spacing in the η direction; in the ξ and ζ directions, the medium grid has greater grid density, especially in the regions near the edges and surface intersections. The third grid, called the fine grid, was derived from the second one by greatly reducing the first grid line spacing from the wing surfaces and increasing the number of points within the expected boundary layer. The distance from the outer boundary to the wing is the same for all three grids. Table 1 summarizes the pertinent features of the grids used in this investigation.

Numerical Procedure

The three-dimensional multizone Navier-Stokes code used in the computations was developed to handle realistic geometries and optimized for modern multiprocessor supercomputers with multiple machine capability. Details about the code and its various applications can be found in Refs. 15–20. Only a summary of the relevant parts of the code pertinent to the calculations reported in this paper is given here.

The governing equations being solved numerically are the full three-dimensional compressible Reynolds-averaged Navier-Stokes equations in their conservation-law forms.[26] Even though there was no tripping wire in the wing model, with the high Reynolds number (6.56×10^6/m) the flow is assumed fully turbulent.[6] Therefore, the coefficient of viscosity in the governing equations μ is calculated from $\mu_L + \mu_T$, where μ_L is given by Sutherland's law and μ_T by the Baldwin-Lomax algebraic turbulence model.[24] Similarly, the coefficient of thermal conductivity k is replaced by $k_L + k_T$, where k_T is given by $c_p\mu_T/Pr_T$. The fluid is assumed thermally and calorically perfect with constant Prandtl numbers having 0.71 and 0.90 as the respective laminar and turbulent values. The transformed governing equations were solved using the origi-

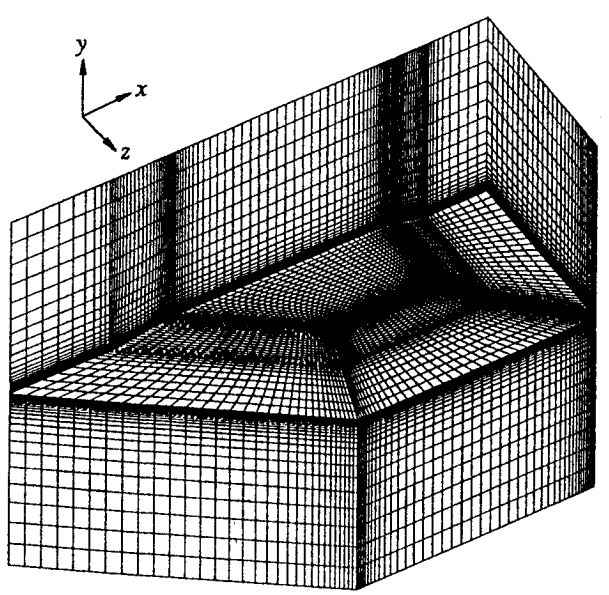

Fig. 3 Overall view of the grid (384,000 total grid points).

nal unsplit predictor/corrector algorithm of MacCormack implemented in finite volume form.[21]

To accelerate the convergence of steady-state calculations, the local time stepping was used. It was accomplished by specifying a constant Courant-Friedrichs-Lewy (CFL) number of 0.9 throughout the computational domain of all four zones. The computation was initialized with a uniform flowfield corresponding to the freestream condition. The computation proceeded in cycles. Within each computational cycle, the calculation for each zone was carried out individually with flow information exchanged between adjacent cells of neighboring zones at the beginning of each cycle. Fictitious boundary cells were used to implement the data transfer.

In order to define the problem properly, suitable numerical boundary conditions must be specified. For the boundary cells at the upstream inflow boundary and the windward side outer boundary, freestream conditions were given for all the flow variables. Along the downstream outflow boundary and the rest of the outer boundaries, zeroth-order extrapolation was used for all the nonconservative variables. At the wing surfaces, no-slip and adiabatic conditions were imposed. Finally, across the symmetry plane, reflection boundary conditions were used.

To account for the wind-tunnel wall and model support interferences effect, in the Navier-Stokes calculation of the transonic flow around two-dimensional airfoils, the actual values of the angle of attack and/or freestream Mach number were adjusted from the test values until the computed lift and drag coefficients matched the test data.[17] In this investigation, the measured values of α and M_∞ were used in the computations without any adjustment in order to reduce the computing cost and time. An additional reason for doing so is that the sting support system used in the wind tunnel test was designed to minimize the sting interference effect on the test data.[23]

The solution was assumed to have reached steady state when the maximum amplitude in the oscillations of the maximum and minimum surface pressure coefficients were < 0.1–0.5%. A more restrictive criterion could be prescribed, but the one described here was found to be adequate for engineering applications. The numerical damping factors used throughout the computation were kept as low as possible without causing numerical instability.

Results and Discussion

Computations were performed corresponding to the wind-tunnel test conditions[23] of $M_\infty = 2.16$, $\alpha = 1.3$, 6.3, and 11.3 deg, and $Re = 1.33 \times 10^6$. The fine, 384,000-point grid was used in all the calculations. The coarse and medium grids were used only for the investigation of the grid resolution effect on the solution at $\alpha = 1.3$ deg. Because of the availability of computing resources and for the purpose of validating the portability of the code, the computations were carried out using a number of computers: Cray XMP, Convex C2, and the Cray 2 supercomputer of the NAS (National Aerodynamic Simulation) Program at NASA Ames Research Center.

A typical computational run for a converged solution using the fine grid took about 1800–2000 iteration steps with a central processor unit (CPU) time of about 25 h on the Cray 2. A computing rate of 13×10^{-5} s/iteration step/grid point was achieved. Since the code was written for general application on a variety of computers, its computing efficiency was lower than that of a code written specifically for one particular prob-

Table 2 Grid effect on computed lift coefficient at $M_\infty = 2.16$ and $\alpha = 1.3$ deg

Grid	Total points	Minimum y^+	C_L Computed	C_L Experimental
Coarse	71,400	2.4	0.0360	
Medium	326,400	2.6	0.0348	0.030
Fine	384,000	0.6	0.0339	

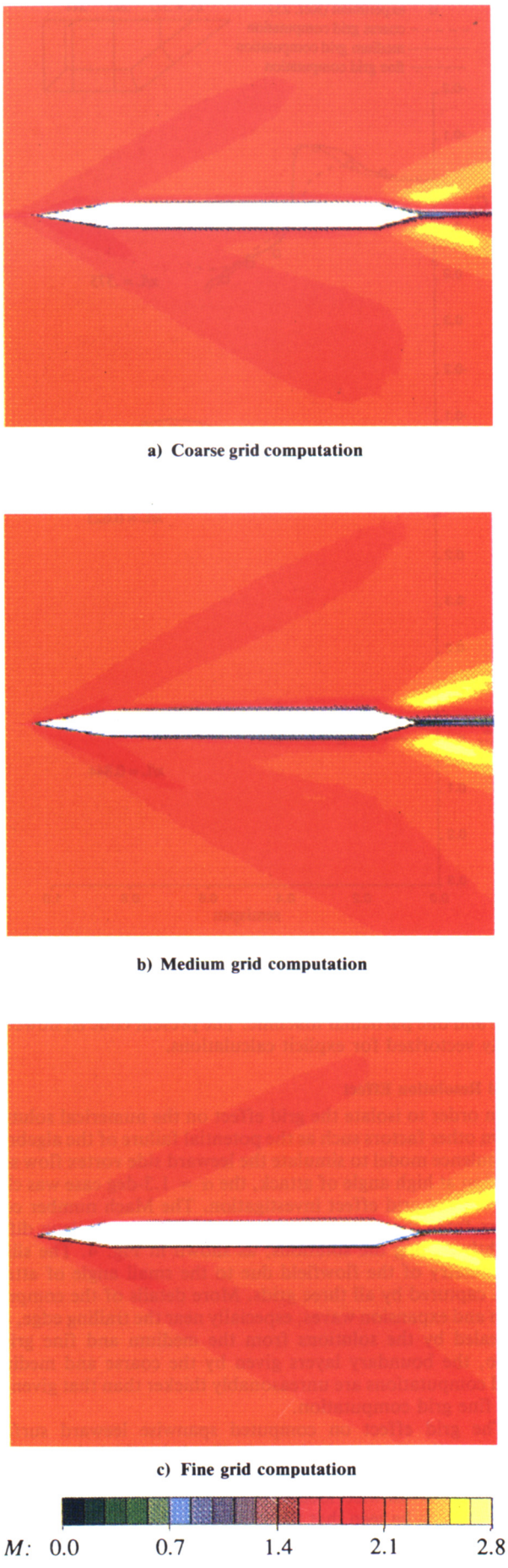

Fig. 4 Grid effect on computed Mach contours on the symmetry plane at $M_\infty = 2.16$ and $\alpha = 1.3$ deg.

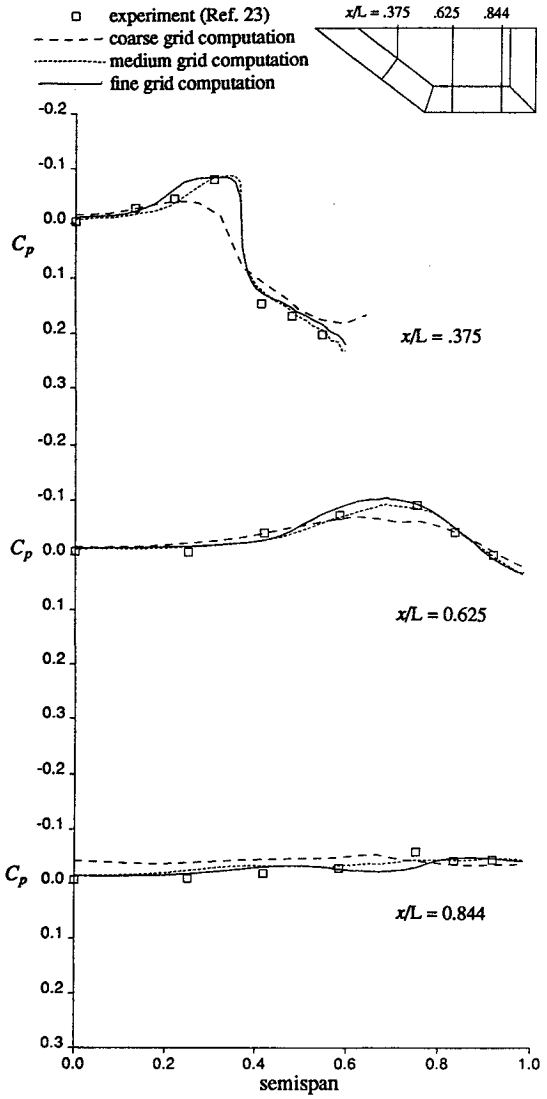

Fig. 5 Grid effect on computed spanwise leeward surface pressure distributions at M_∞ = 2.16 and α = 1.3 deg.

lem and one particular machine. The present code is, however, fully vectorized for explicit calculations.

Grid Resolution Effect

In order to isolate the grid effect on the numerical solution from other factors such as the potential failure of the algebraic turbulence model to simulate the leeward side vortex flow separation at high angle of attack, the α = 1.3-deg case was chosen for the grid effect investigation. The Mach number contours from the different grids on the symmetry plane differ slightly among the solutions, as shown in Fig. 4. The slight asymmetry of the flowfield due to the small angle of attack was captured by all three grids. More details of the compression and expansion waves, especially near the trailing edge, are revealed by the solutions from the medium and fine grids. Also, the boundary layers given by the coarse and medium grid computations are unreasonably thicker than that given by the fine grid computation.

The grid effect on computed spanwise leeward surface pressure distributions is shown in Fig. 5, in which the pressure coefficient C_p is compared with the experimental data at three different streamwise locations of x/L = 0.375, 0.625, and 0.844. It can be seen that the increase in the grid point clustering density around the surface intersections greatly improves the solution accuracy. The solutions from both the medium and fine grids closely match the wind-tunnel test data. Since the angle of attack is very small, the computed and experimental windward surface pressure distributions are very close to those of the leeward side, and the grid effects on them are also similar.

The comparison of the computed lift coefficients, C_L, with the experimental data is summarized in Table 2. Again, great improvement was obtained due to the grid refinement between the medium and coarse grids. The typical distance from the first grid line to the leeward side surface at midchord location in all three grids is also listed in Table 2 in terms of the law-of-the-wall coordinate y^+.

The improvement in the computed surface pressure distributions and the lift coefficient due to the fine grid over the

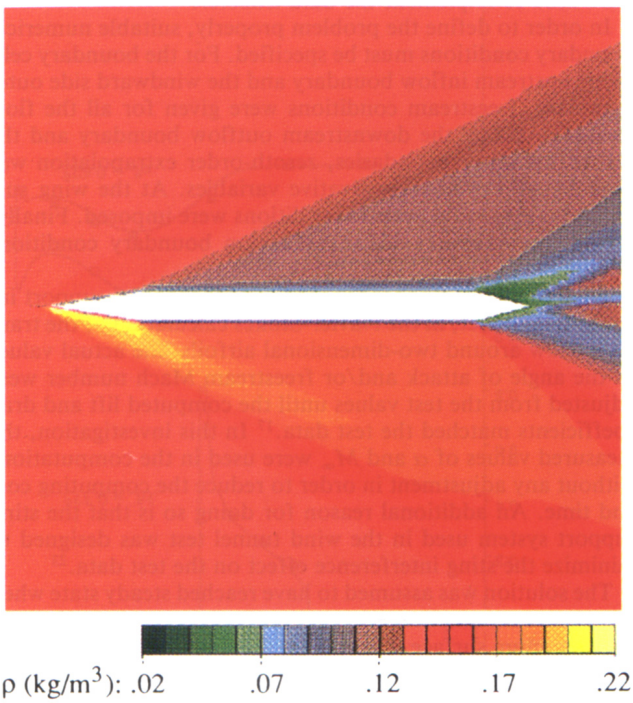

Fig. 6 Density contours on the symmetry plane at M_∞ = 2.16 and α = 6.3 deg.

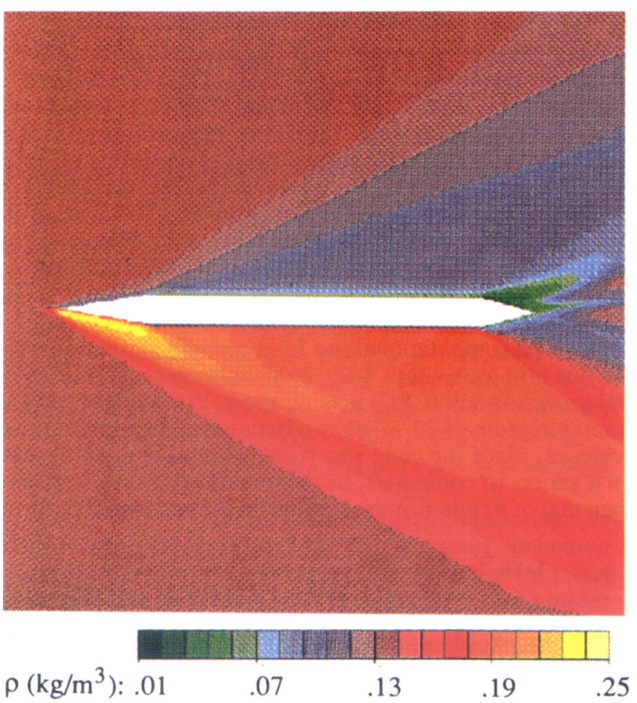

Fig. 7 Density contours on the symmetry plane at M_∞ = 2.16 and α = 11.3 deg.

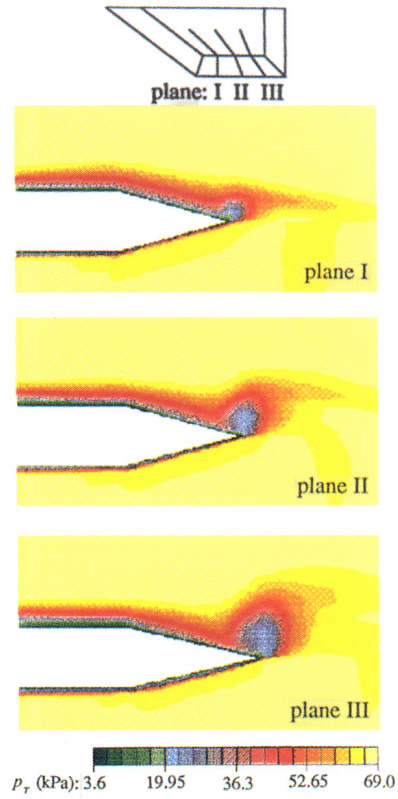

Fig. 8 Total pressure contours on selected cross planes at M_∞ = 2.16 and α = 6.3 deg.

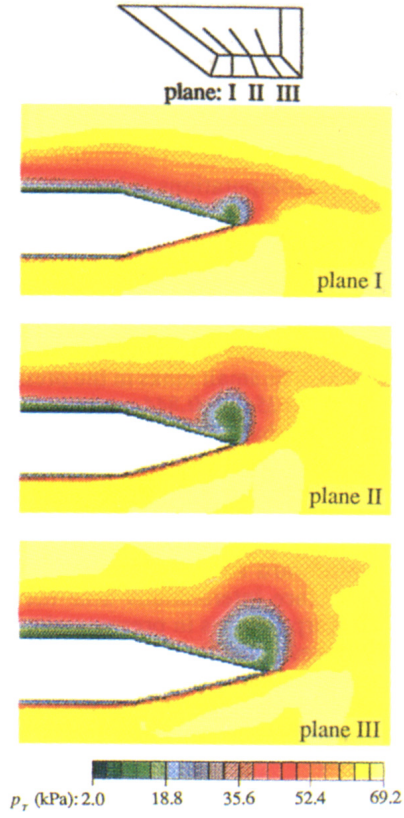

Fig. 9 Total pressure contours on selected cross planes at M_∞ = 2.16 and α = 11.3 deg.

medium one is small. However, for vortex flow, a very fine grid resolution in the region immediately adjacent to, and in certain regions away from, the solid surface is necessary to capture the flow details there,[10,11] especially at higher angle of attack when the vortex flow and vortex induced separation are dominant. Therefore, the fine grid was used for all subsequent calculations at higher angles of attack.

Solutions at α = 6.3 and 11.3 deg

The calculations for flows at α = 6.3 and 11.3 deg were performed using the fine grid on a Convex C2 minisupercomputer. Figures 6 and 7 show the density contours on the symmetry plane at α = 6.3 and 11.3 deg, respectively. The detail of the expansion and compression waves at the leading and trailing edges and at the surface intersections is clearly shown by the contours. Comparing with the flowfield at α = 1.3, the more pronounced asymmetry of the flowfields at higher angles of attack is very well demonstrated.

The expected leeward-side vortical crossflows, even at moderate angles of attack, are shown in Figs. 8 and 9 in terms

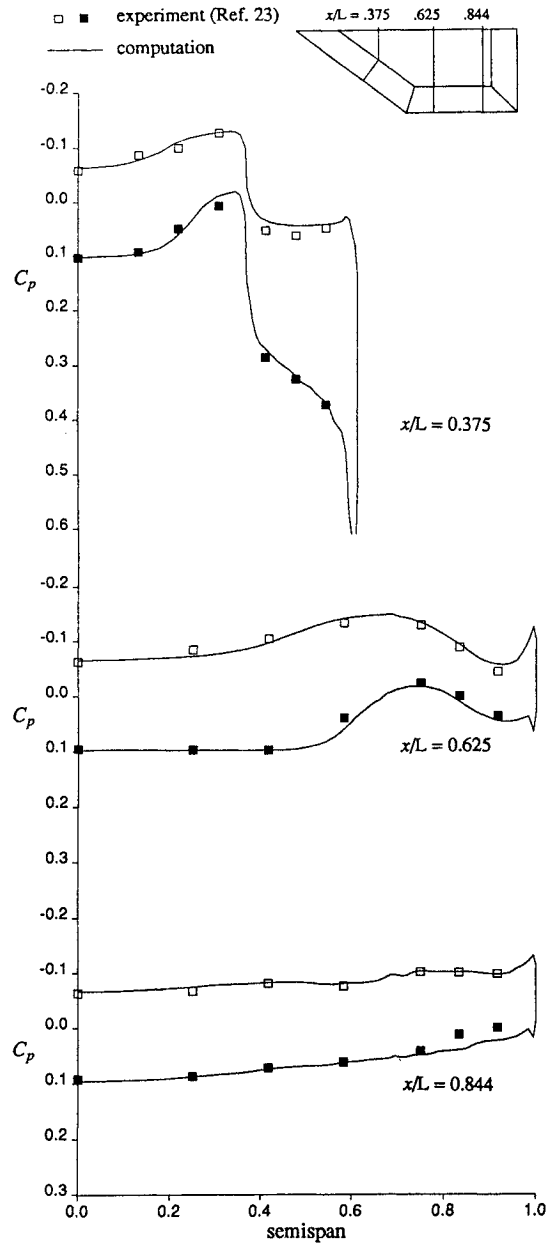

Fig. 10 Comparison of computed and experimental spanwise surface pressure distributions at M_∞ = 2.16 and α = 6.3 deg.

of the spanwise total pressure contours on three selected cross planes. The presence of the vortical flows is clearly shown for both cases. The strength of the vortices increases as a function of angle of attack α; at a fixed α it increases from planes I to III with increasing distance downstream from the apex. Apparently, with a sufficiently refined grid and at low-to-moderate angles of attack, the vortical flowfield can be simulated adequately, even using the simple Baldwin-Lomax turbulence model. Although it is recognized that a more complex turbulence model is required for the detailed simulation of vortex flows, the present results suggest that modeling problems frequently attributed to inadequate turbulence modeling often may be due to the use of an inadequate grid resolution.

It appears that the phenomena of vortex-breakdown and secondary vortex formation were not shown by the calculation, probably due to the low angle of attack and low leading-edge swept angle. Furthermore, the expansion due to the existence of the slanting surfaces near the trailing and side edges may delay or even prevent the breakdown of the vortex. To resolve this uncertainty, computations at higher angles of attack are necessary.

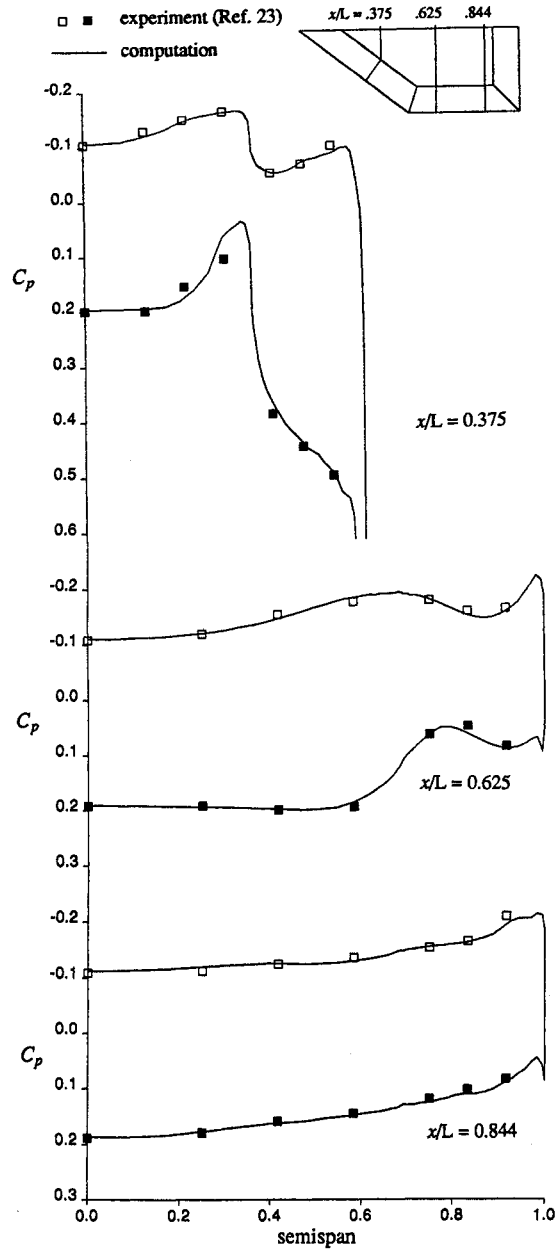

Fig. 11 Comparison of computed and experimental spanwise surface pressure distributions at $M_\infty = 2.16$ and $\alpha = 11.3$ deg.

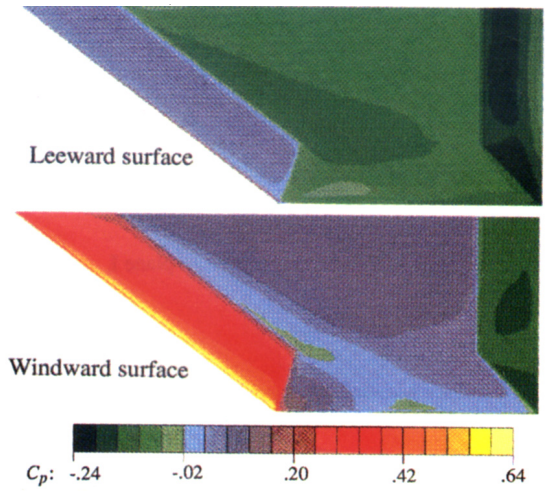

Fig. 12 Pressure contours at $M_\infty = 2.16$ and $\alpha = 6.3$ deg.

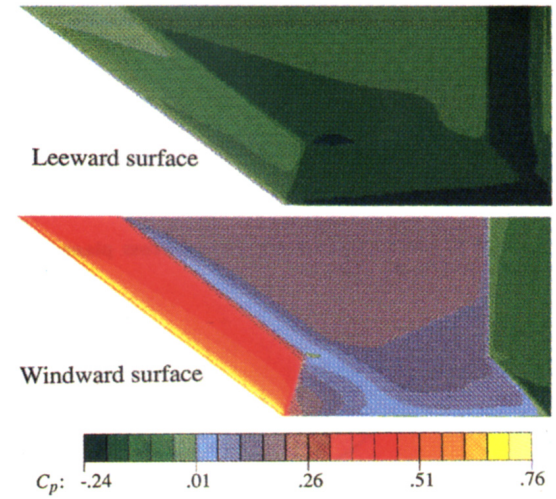

Fig. 13 Pressure contours at $M_\infty = 2.16$ and $\alpha = 11.3$ deg.

The comparisons of the computed spanwise surface pressure distributions with the wind-tunnel test data are shown in Figs. 10 and 11, for $\alpha = 6.3$ and 11.3 deg, respectively, at three streamwise locations: $x/L = 0.375$, 0.625, and 0.844. For both cases, very good agreement between the computation and test was achieved. The small kinks in the pressure distribution curves at $x/L = 0.625$ and 0.844 are probably due to the numerics because of the sharp edge between the flat and slanting surfaces at the semispan location of 0.69.

The surface pressure contours for $\alpha = 6.3$ and 11.3 deg are shown in Figs. 12 and 13, respectively. The contours, expressed in terms of the pressure coefficient C_p are shown on the leeward and windward surfaces for both cases. Over the flat and slanting surface intersections near the leading and trailing edges, the sharp changes in pressure, clearly shown by the contours, are the results of the compression and expansion waves there. Over the similar surface intersection near the side edge, the pressure change is much less drastic because the crossflow is only secondary in comparison with the flow in the streamwise direction.

The computed lift coefficients are compared with the experimental data in Table 3. It can be seen that the agreement between the computation and experiment is very good. It should be pointed out that a good agreement between calculated and experimental lift coefficients can be obtained

Table 3 Comparison of computed and experimental lift coefficients at $M_\infty = 2.16$

α, deg	Grid	Minimum y^+	C_L Computed	C_L Experimental
6.3	Fine	0.5	0.168	0.164
11.3	Fine	0.5	0.306	0.308

without a corresponding match in surface pressure distributions. Without the latter, the former cannot be used alone as the criterion for code validation.

Conclusions

A Navier-Stokes code has been applied to supersonic viscous flow around a delta-rectangular wing with slanting surfaces at low-to-moderate angles of attack. Computational results are in very good agreement with experimental data. The multizone capability of the code is essential in solving flow problems involving complex and realistic geometries. Over the range of angles of attack considered in this investigation, the simple Baldwin-Lomax algebraic turbulence model is capable of simulating the leeside vortical flows. The slanting surfaces of the wing may be one of the contributing factors to the lack of observing vortex breakdown, and additional calculations at higher angles of attack are necessary for a clearer understanding. A more sophisticated turbulence model may then be required. A sufficiently refined grid is needed regardless of the turbulence model used in order to generate credible numerical results. Matching computation with test data both in lift coefficients and surface pressure distributions is essential in any code validation. Substantial reduction in computing cost is expected when the implicit algorithm option of the code, currently being implemented, is used.

Acknowledgments

This work was supported by the Boeing Independent Research and Development program. The author wishes to thank the members of the Computational Fluid Dynamics Group of Aerodynamics/Hydrodynamics & Acoustics, Boeing Aerospace & Electronics for their cooperation and help. The usage of the Cray 2 computer and the computational supporting facilities of the Numerical Aerodynamic Simulation program at NASA Ames Research Center is gratefully acknowledged.

References

[1]Hummel, D., "On the Vortex Formation over a Slender Wing at Large Angles of Incidence," AGARD CP-247, Feb. 1983.

[2]Ayoub, A., and McLachlan, B. G., "Slender Delta Wing at High Angles of Attack—A Flow Visualization Study," AIAA Paper 87-1230, June 1987.

[3]Freymuth, P., Finaish, F., and Bank, W., "Further Visualization of Combined Wing Tip and Starting Vortex Systems," *AIAA Journal,* Vol. 25, No. 9, 1987, pp. 1153–1159.

[4]Payne, F. M., Ng, T. T., and Nelson, R. C., "Visualization and Wake Surveys of Vortical Flow over a Delta Wing," *AIAA Journal,* Vol. 26, No. 2, 1988, pp. 137–143.

[5]Thomas, J. L., Taylor, S. L., and Anderson, W. K., "Navier-Stokes Computations of Vortical Flows over Low Aspect Ratio Wings," AIAA Paper 87-0207, Jan. 1987; see also *AIAA Journal,* Vol. 28, No. 2, 1990, pp. 205–213.

[6]McMillin, S. N., Thomas, J. L., and Murman, E. M., "Euler and Navier-Stokes Solutions for the Leeside Flow over Delta Wings at Supersonic Speeds," AIAA Paper 87-2270, Aug. 1987.

[7]Sirbaugh, J. R., "Euler Analysis of the AFWAL 65-degree Delta Wing," AIAA Paper 87-2272, Aug. 1987.

[8]Rizzi, A., Müller, B., and Purcell, C. J., "Comparison of Euler and Navier-Stokes Solutions for Vortex Flow over a Delta Wing," AIAA Paper 87-2347, Aug. 1987.

[9]Frink, N. T., "Computational Study of Wind-Tunnel Effects on Flow Field Around Delta Wing," AIAA Paper 87-2420, Aug. 1987.

[10]Fujii, K., and Schiff, L. B., "Numerical Simulation of Vortical Flows over a Strake-Delta Wing," AIAA Paper 87-1229, June 1987.

[11]Fujii, K., Gavali, S., and Holst, T. L., "Evaluation of Navier-Stokes and Euler Solutions for Leading-Edge Separation Vortex," NASA TM-89458, 1987.

[12]Hsu, C.-H., Hartwich, P.-M., and Liu, C. H., "Computation of Vortical Interaction for a Sharp-Edged Double-Delta Wing," *Journal of Aircraft,* Vol. 25, No. 5, 1988, pp. 442-447.

[13]Hitzel, S. M., "Wing Vortex-Flows Up Into Vortex-Breakdown," AIAA Paper 88-2518, June 1988.

[14]Kandil, S. A., and Chuang, H. A., "Unsteady Delta-Wing Flow Computation Using an Implicit Factored Euler Scheme," AIAA Paper 88-3649, June 1988.

[15]Hopcroft, R. G., "Structuring Computational Fluid Dynamics Analysis Systems," *Proceedings of the Third International Conference on Numerical Methods in Laminar and Turbulent Flow,* edited by C. Taylor, J. A. Johnson, and W. R. Smith, Pineridge Press, Swansea, Wales, UK, Aug. 1983, pp. 1173–1183.

[16]Hoffman, J. J., Birch, S. F., Hopcroft, R. G., and Holcomb, J. E., "Navier-Stokes Calculations of Rocket Base Flows," AIAA Paper 87-0466, Jan. 1987.

[17]Chan, J. S., "Multizone Navier-Stokes Computations of Viscous Transonic Flows Around Airfoils," AIAA Paper 88-0103, Jan. 1988.

[18]Warfield, M. J., "Calculation of Supersonic Interacting Jet Flows," AIAA Paper 89-0666, Jan. 1989.

[19]Hoffman, J. J., "Development of an Algorithm for the Three-Dimensional Fully-Coupled Navier-Stokes Equations with Finite Rate Chemistry," AIAA Paper 89-0670, Jan. 1989.

[20]Holcomb, J. E., "Three-Dimensional Navier-Stokes Rocket Plume Calculations," AIAA Paper 89-1986, June 1989.

[21]MacCormack, R. W., "The Effect of Viscosity in Hypervelocity Impact Cratering," AIAA Paper 69-0354, May 1969.

[22]MacCormack, R. W., "Current Status of Numerical Solutions of the Navier-Stokes Equations," AIAA Paper 85-0032, Jan. 1985.

[23]Stallings, R. L., Jr., and Lamb, M., "Wing-Alone Aerodynamic Characteristics for High Angles of Attack at Supersonic Speeds," NASA TP-1889, 1981.

[24]Baldwin, B. S., and Lomax, H., "Thin Layer Approximation and Algebraic Model for Separated Turbulent Flows," AIAA Paper 78-0257, Jan. 1978.

[25]Holcomb, J. E., "Development of a Grid Generator to Support 3-D Multizone Navier-Stokes Analysis," AIAA Paper 87-0203, Jan. 1987.

[26]Anderson, D. A., Tannehill, J. C., and Pletcher, R. H., *Computational Fluid Mechanics and Heat Transfer,* McGraw-Hill, New York, 1984, pp. 480–481.

Walter B. Sturek
Associate Editor